Experimental Study of the Uniaxial Stress-strain Relationships of Parallel Strand Bamboo in the Longitudinal Direction

Baolu Sheng,[a,b,]* Yuling Bian,[c] Yanyan Liu,[b] Ying-Hei Chui,[d] and Aiping Zhou [b]

Parallel strand bamboo has extensive potential applications as a structural material for construction. Studying longitudinal stress-strain relationships is essential as a means to build a constitutive law for parallel strand bamboo composites and to conduct an inelastic analysis for structural members constructed by this material. For this reason, failure modes and the damage mechanisms were investigated for tension and compression in parallel strand bamboo composites in the longitudinal direction. An analytical stress-strain formula for the parallel strand bamboo composites was developed for tension and compression related calculations. Tensile failure was caused by the damage of the longitudinal fibers and showed brittle characteristics. The compressive failure resulted from the buckling of the fibers near the damage area. In addition, three types of failure modes were observed; longitudinal buckling failure, compressive-shearing failure, and longitudinal crush failure. The stress-strain relationship in the longitudinal direction of parallel strand bamboo composites exhibited linear behaviour for tension. However, the stress-strain relationship for compression remained linear within the proportional limit, while becoming nonlinear, which can be simulated by a quadratic polynomial, once the stress exceeded the limit. The experimental data agreed well with the model predictions, showing that the present model had high prediction accuracy.

Keywords: Parallel strand bamboo; Uniaxial stress-strain relationship; Failure mode; Failure mechanism

Contact information: a: School of Civil Engineering, Nanjing Forestry University, Nanjing 210037, China; b: National Engineering Research Center of Biomaterials, Nanjing Forestry University, Nanjing 210037, China; c: Wuxi institute of commerce, Wuxi 214000, China; d: Department of Civil and Environment Engineering, University of Alberta, Edmonton, T6G 1H9, Canada;
** Corresponding author: baolu52520@163.com*

INTRODUCTION

Parallel strand bamboo (PSB) is a high-strength bamboo-based composite, which is manufactured by gluing together parallel aligned strands of bamboo with PF resin in the longitudinal direction under high pressure. The mechanical properties and flame-retardant properties are superior to those of lumber, and PSB has lower carboxaldehyde emissions than required for an E1 grade according to EU standards. The fabrication methodology and technology for PSB has been standardized after nearly 30 years of research and development. The PSB is created *via* current fabrication methods with ultimate tensile and compression strength of 160 MPa and 140 MPa in the longitudinal (parallel-to-grain) direction, respectively. The modulus of the PSB in the longitudinal direction reached 14,000 MPa (Huang *et al.* 2013); PSB composites fabricated *via* industrial processes have consistent properties and stable mechanical behaviors, and they can be made into various shapes and sizes according to the application requirements. The moisture content of PSB composites is less than 12%, resulting in less likelihood of failure (shrinkage, warping, cupping, bowing, or splitting) comparing to the unmodified bamboo. In the past two decades, PSB composites have been widely used for flooring, furniture, and other decoration materials. Recently, this material has garnered attention into its application in construction.

After the May 12^{th} Wenchuan earthquake, some scholars in China began to utilize PSB composites in building structures. Some modern bamboo structure systems, such as light bamboo structures (Xiao *et al.* 2009; Gou *et al.* 2011a,b; Xiao and Ma 2012), hybrid steel-bamboo structures (Li *et al.* 2012), and PSB frame structures (Zhou *et al.* 2012), were developed. Demo houses using prefabricated PSB frame structures were constructed on the Nanjing Forestry University campus, as well as in Qingchuan (Sichuan province), where they were severely damaged in the May 12^{th} earthquake (Wei *et al.* 2011; Zhou *et al.* 2012). Engineering practices showed that PSB structures were superior to other traditional building structures in terms of economics, safety, and standardized construction. It is easy for PSB components to be carried and installed due to their lightweight characteristics, and they are especially suitable for rapid constructability, since PSB buildings can be constructed through dry operation. No special skills are needed for building PSB structures, and the safety of the structures can be guaranteed, since the structure members are designed and fabricated by manufacturers.

The fibers of PSB composites are parallel to each other in the longitudinal (parallel-to-grain) direction, while they are uniformly distributed in the transverse (perpendicular-to-grain) direction. Therefore, the mechanical properties of PSB are obviously oriented (Chung *et al.* 2002; Lo *et al.* 2004, 2008; Huang *et al*. 2010). Consequently, PSB is an oriented fiber-reinforced biocomposite. The mechanical performance of PSB in the longitudinal direction is distinct from its performance in the transverse direction. Even the tensile and compressive properties in the same direction are significantly different from each other. The compressive stress-strain relationship in the longitudinal direction of PSB composites exhibits significant nonlinearity (Huang *et al.* 2013; Chen *et al*. 2015). Therefore, the load-deformation relations of the PSB components consequently exhibit nonlinearities once the stress approaches or reaches the limit of the load-carrying capacity. Consideration of the nonlinear properties of materials in structural design is a fundamental requirement of the ultimate probability state design philosophy. Nonlinear analysis of the maximum load-carrying capacity for traditional structures, such as concrete and steel structures, are well developed; however, they are not suitable for the nonlinear analysis of PSB structures, since there are significant differences in the constitutive relations and the failure mechanisms between PSB and traditional materials. The load-carrying capacity and ultimate deformation of PSB components in current engineering practices were obtained *via* direct experimentation (Lu *et al.* 2008; Wei e*t al*. 2010). For this reason, establishing the nonlinear stress-strain relationships of PSB composites is essential for the nonlinear analysis of PSB components.

PSB composites were first fabricated in China 30 years ago, and the influence of manufacturing processes on its physical properties has been fully studied (Li *et al.* 2001; Xiao *et al*. 2005; Li *et al*. 2009; Chun 2016). However, a fundamental investigation of its mechanical behaviors, aimed at developing a design philosophy and structural analysis theory for PSB, has not been conducted, and the failure mechanisms of PSB composites are not well understood. A constitutive law or a nonlinear analysis approach for PSB components under the ultimate state has not been developed.

This paper idealized PSB as an orthotropic and transversely isotropic composite. Parallel-to-grain and perpendicular-to-grain directions for this composite were defined as longitudinal and transverse, respectively. The damage modes for tension and compression in the longitudinal direction were studied *via* experimentation. The failure mechanisms of the corresponding damage modes were investigated, and an analytical stress-strain formula for PSB composites was established.

EXPERIMENTAL

Testing Methods

Five-year-old *Phyllostachys pubesens*, a bamboo species commonly harvested in southeast China, was selected to fabricate the experimental material from Guangde, Anhui province, China. Considering that the mechanical properties and the thickness of raw bamboo are varied along the longitudinal direction of the culm, the authors divided the bamboo culm into three 1900 mm long sections from top to bottom. The test materials were manufactured according to ASTM D143 (2014) with dimensions of 25 mm x 5 mm x 453 mm. Experimental methodology referred to the relative items of ASTM D143 (2014) because there are no test standards for PSB composites or their components available currently. Figure 1 presents the size and shape of specimens for the tensile tests. Prisms with dimensions of 50 mm x 50 mm x 200 mm were chosen as the specimens for the compressive tests (as shown in Fig. 2).

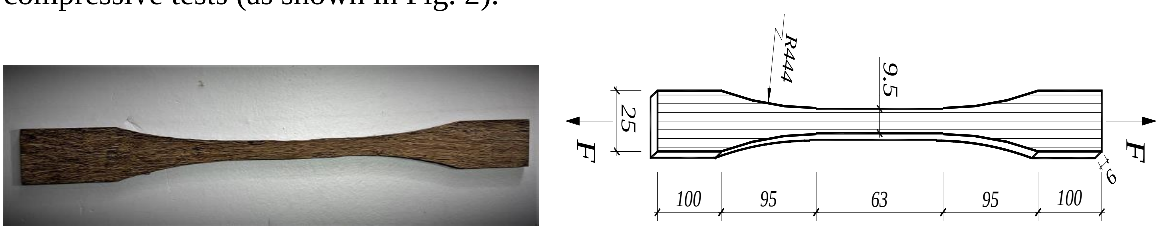

Fig. 1. Tensile specimen (mm)

Fig. 2. Compressive specimen (mm)

The dimensions of the effective parts of the specimens were measured three times and averaged before testing. Strain gauges were glued in the middle of the specimens along the longitudinal direction. The strains, loads, and elongations corresponding to each loading step were recorded simultaneously at a frequency of 1 Hz by a TDS-530 strain acquisition instrument (Shenzhen SANS Testing Machine Co., Ltd, Shenzhen, China). An MTS servo-dynamic loading system (Earth Products China Limited (EPC), Guangzhou, China) was utilized to apply the load to the specimens. In order to eliminate the gaps between the grips and the specimens, a two-time loading and unloading cycle at a range of 0 kN to 5 kN with a rate of 1 kN/min were conducted before the test.

The loading and unloading cycles were repeated within a range of 2 kN to 4 kN six times at a rate of 0.8 kN/min for the tensile properties test. Loading values and strains were recorded simultaneously from the beginning to the end. The data obtained from the final four cycles were used to calculate the average values of longitudinal Young's modulus with Eq. 1,

$$E_t = \frac{\Delta F_t}{bt\Delta\varepsilon_t} \tag{1}$$

where E_t is the tensile moduli of bamboo in the longitudinal direction (MPa), $\Delta\varepsilon_t$ is the increment of strain in the middle section along the longitudinal direction ($\mu\varepsilon$), ΔF_t is the increment of loading (*k*N), *b* is the width of the middle section (mm), and *t* is the thickness of the middle section (mm).

Uniform force was applied, which was controlled by the displacement of machine head at a rate of 0.1 mm/min until the specimen collapse. The load-displacement curves and the longitudinal strain in the whole process of testing were recorded simultaneously. The tensile strength of the specimen may be estimated with Eq. 2,

$$\sigma_u = \frac{F_u}{bt} \tag{2}$$

where σ_u is the tensile strength of test material (MPa), F_u is the maximum load applied to the specimen (*k*N), *b* is the width of the middle section (*mm*), and *t* is the thickness of the middle section (*mm*).

Strain gauges were longitudinally glued in the middle of each side surface for the four compressive specimens. The loading method for the compression test was the same as the test for the tensile specimens. Similarly, the loading forces, the strains, and the stretch value of the specimens were recorded simultaneously. The compressive moduli was calculated using Eq. 3,

$$E_c = \frac{\Delta F_c}{A\Delta\varepsilon_c} \tag{3}$$

where E_c is the compressive moduli of bamboo in the longitudinal direction (mm), $\Delta\varepsilon_c$ is the increments of strain in the middle section along the longitudinal direction ($\mu\varepsilon$), ΔF_c is the increment of loading (*k*N), F_c is the maximum load applied to the specimen (*k*N), and A is the area of the corresponding cross-section (mm^2).

The strength of the specimen was calculated using Eq. 4,

$$\sigma_c = \frac{F_c}{A} \tag{4}$$

where σ_c is the compressive strength of test material (MPa), F_c is the maximum load applied to the specimen (*k*N), and A is the area of corresponding cross-section (mm^2).

RESULTS AND DISCUSSION

Test Phenomenon

The stress-strain relationship exhibited perfect linear behavior from loading to failure during the tensile test. Brittle breakage of the specimens took place once the tensile load reached the maximum value. A typical stress-strain relationship and three compression failure modes are shown in Fig. 3 and Fig. 4, respectively.

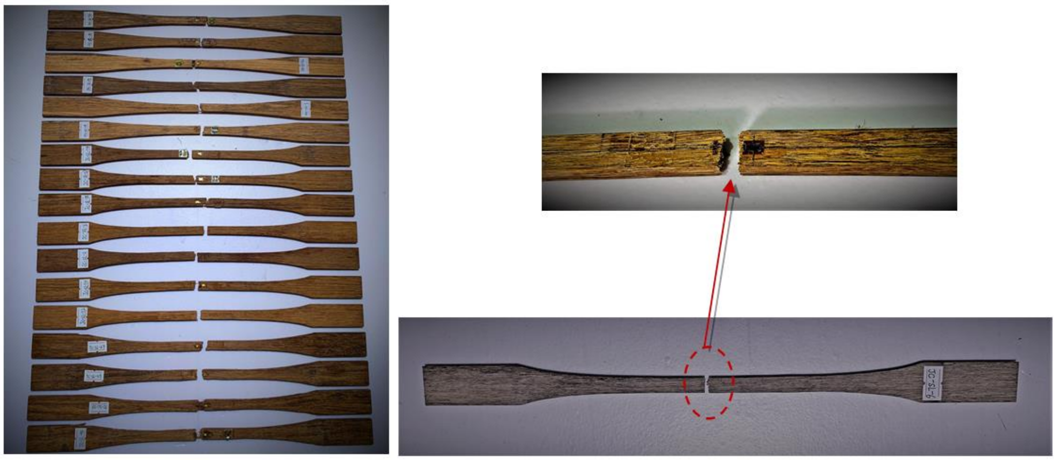

Fig. 3. A broken tensile specimen

Three principle failure modes during the compressive test were observed. The first, mode 1, was a buckling failure in the longitudinal direction. The failure mechanism can be explained as follows; initially, no damage took place in the specimen, and the stress was linearly distributed relative to the change in strain. With further loading, primary cracks were observed on the surface of the specimen in a parallel to grain direction, whereas the stress was still linearly distributed with respect to the change in strain. Once the load reached approximately 70% of the maximum value, these cracks gradually propagated and gathered along the grain direction of the material with the increase in compressive load. The specimen consequently developed one or more secondary fracture surfaces throughout the specimen, which divided the prism into several sub-columns. As a result, the stress-strain curve turned into nonlinear behavior, and the specimen was crushed to failure with the broken fibers forming in the longitudinal direction, as shown in Fig. 4a. Mode 2 showed shear failure under a compressive load. Later in the compressive testing period, a 45° angle diagonal crack formed through the specimen in the loading direction, which could be observed in surfaces perpendicular to the grain of the material. With an increase in compressive force, the fibers gradually buckled along the diagonal crack and consequently developed a slipping shear surface along the crack, leading the specimen to failure. A typical mode 2 failure is shown in Fig. 4b. Mode 3 was a splitting failure in the parallel to grain direction and is shown in Fig. 4c. Later in the compressive testing period, several longitudinal fine cracks emerged in the specimen along two diagonal lines, which formed a V-shaped line in the surfaces perpendicular to the grain of the material. These cracks were gradually expanded along the V-shaped lines due to the fibers across the cracks buckling under the increased compressive load. The prism was finally divided into two parts by the V-shaped lines. The upper part was crushed into the lower part of the specimen along the V-shaped line, and the prism consequently failed.

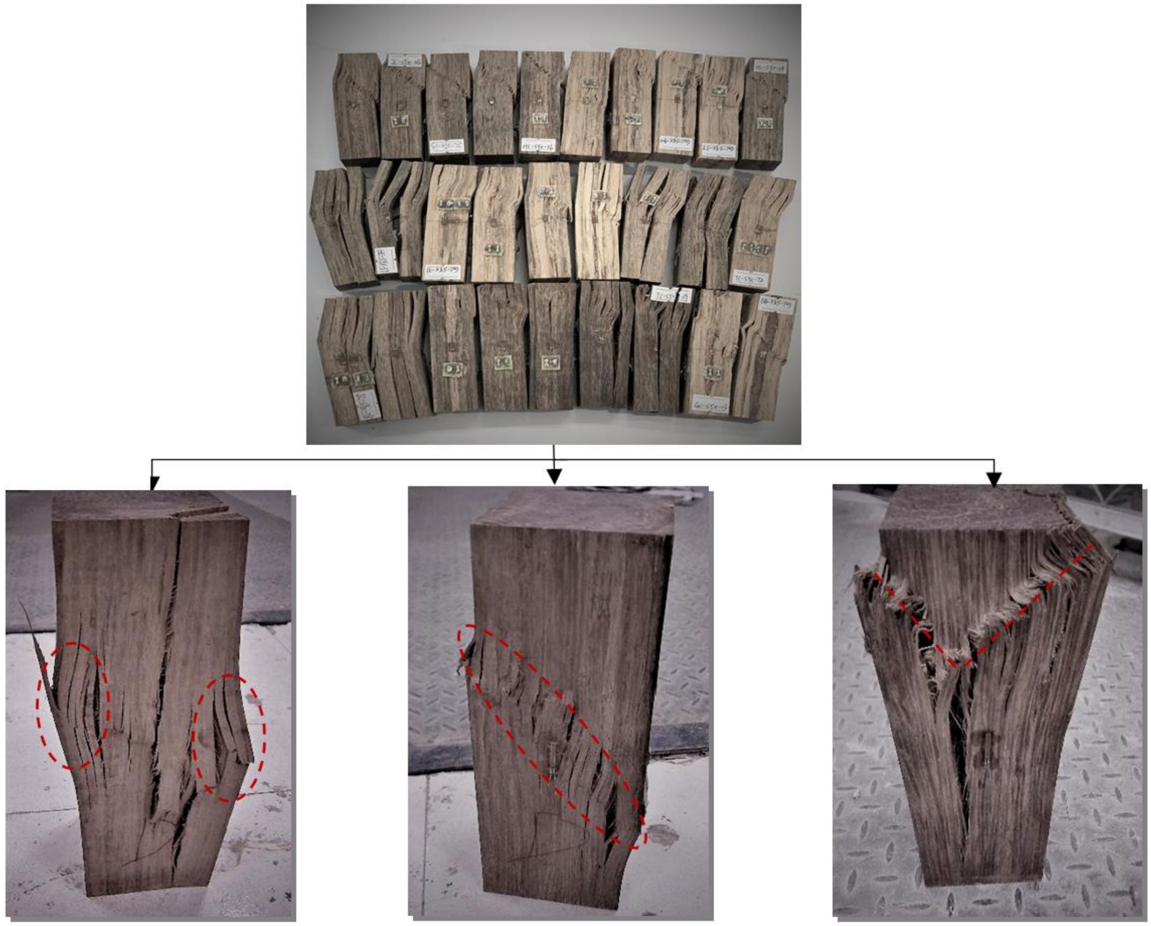

Fig. 4. Compression failure modes

A failure initiated by the expansion of longitudinal cracks and the buckling of fibers across this crack were common characteristics between the three failure modes observed. Therefore, there was essentially no difference between the three failure modes. The stress-strain relationship can approximately be divided into two stages, as shown in Fig. 5. The first stage represented linear behavior; however, once the load reached approximately 70% of the maximum value, the curve turned to nonlinear behavior for the second stage.

Test Results

The results of the tensile and the compressive experiments are shown in Tables 1 and 2, respectively. The stress and strain values were divided into seven intervals, and the frequencies at which the values fell into each interval are illustrated in Table 1. The values that fall into these intervals at higher frequencies and were continuously distributed were used for statistical analysis, as shown by a grey background in Table 1. Statistical analysis of the moduli is shown in Table 2, and results of both statistical analyses are shown in Table 3.

Table 1. Statistical Analysis of the Stress and Strain Test Values

Maximum Tensile Limit				Proportional Compressive Limit				Maximum Compressive Limit			
Stress (MPa)	Freq	Strain ($\mu\varepsilon$)	Freq	Stress (MPa)	Freq	Strain ($\mu\varepsilon$)	Freq	Stress (MPa)	Freq	Strain ($\mu\varepsilon$)	Freq
75.78 to 91.96	1	7853 to 8917	2	27.47 to 31.22	4	3119 to 3558	2	41.12 to 44.73	3	9265 to 13659	2
91.96 to 108.13	5	6789 to 7853	8	31.22 to 34.98	1	3558 to 4036	1	44.73 to 48.34	1	13659 to 18053	6
108.13 to 124.31	2	8917 to 9981	4	34.98 to 38.73	2	4036 to 4494	1	48.34 to 51.95	5	18053 to 22447	3
124.31 to 140.49	7	9981 to 11045	8	38.73 to 42.48	9	4494 to 4952	6	51.95 to 55.55	6	22447 to 26841	6
140.49 to 156.67	6	11045 to 12109	6	42.48 to 46.23	9	4952 to 5410	8	55.55 to 59.16	5	26841 to 31236	6
156.67 to 172.84	6	12109 to 13173	7	46.23 to 49.99	2	5410 to 5868	7	59.16 to 62.77	3	31236 to 35630	4
172.84 to 189.02	6	13173 to 14237	1	49.99 to 53.74	1	5868 to 6326	2	62.77 to 66.38	7	35630 to 40024	1

Thus, the tensile and compressive properties of PSB composites were significantly distinct; (1) the stress-strain relationship of PSB composites exhibited full linear behaviour under tension; however, under compression it exhibited a linear and nonlinear hardening stage before and after the proportional limit; (2) the tensile and the compressive moduli of PSB composites were essentially identical; however, the tensile strength was far greater than the compressive strength, and the maximum strain value of tension was much higher than that of compression.

Table 2. Statistical Analysis of Test Moduli

Tensile Moduli		Compressive Moduli	
Interval (GPa)	Freq	Interval (GPa)	Freq
9.77 to 11.26	5	10.80 to11.58	4
11.26 to 12.75	9	11.58 to12.36	4
12.75 to 14.25	12	12.36 to13.14	5
14.25 to 15.74	6	13.14 to13.92	4
15.74 to17.23	1	13.92 to 14.00	3

Table 3. Statistics Results

Value	Maximum Tensile Limit		Proportional Compressive Limit		Maximum Compressive Limit		Tensile Moduli (GPa)	Compressive Moduli (GPa)
	Stress (MPa)	Strain ($\mu\varepsilon$)	Stress (MPa)	Strain ($\mu\varepsilon$)	Stress (MPa)	Strain ($\mu\varepsilon$)		
Mean	144.27	12509	42.07	5204	58.31	28764	13.29	12.72
STD	12.91	1300	2.53	345	5.40	4035	1.09	1.10
CV	8.9%	10.4%	6.01%	6.6%	9.3%	14.0%	8.16%	8.60%

Uniaxial Stress-Strain Relationships

The gray line in Fig. 5a shows the test curves of the stress-strain relationships of the PSB composites. The longitudinal stress-strain relationships of the PSB composites under uniaxial loading can be simulated as lines, as shown in Fig. 5b. The nonlinear behavior of the compressive stress-strain relationship of the PSB composites can be simulated *via* quadratic polynomial through the numerical fitting of the test results. Hence, the uniaxial longitudinal stress-strain relationships of the PSB composites can be represented as a piecewise function as shown in Eq. 5,

$$\sigma(\varepsilon) = \begin{cases} a_1(\varepsilon + a_2)^2 + a_3 & -\varepsilon_{\mathrm{cu}} \le \varepsilon \le -\varepsilon_{\mathrm{ce}} \\ E_c\varepsilon & -\varepsilon_{\mathrm{ce}} \le \varepsilon \le 0 \\ E_t\varepsilon & 0 \le \varepsilon \le \varepsilon_{\mathrm{tu}} \end{cases} \tag{5}$$

where a_i (i = 1, 2, 3) are coefficients, E_c is the compressive moduli of bamboo in the longitudinal direction (*mm*), E_t is the tensile moduli of bamboo in the longitudinal direction (MPa), ε_{tu} and ε_{cu} are the maximum strain in the tensile and compressive loading, respectively ($\mu\varepsilon$), and ε_{ce} is the compressive strain at the point of proportional limit ($\mu\varepsilon$). Considering the continuous conditions of the stress-strain curves gives Eq. 6a, 6b, and 6c,

$$\sigma(\varepsilon_{\mathrm{ce}}) = a_1\varepsilon_{\mathrm{ce}}^2 + 2a_1a_2\varepsilon_{\mathrm{ce}} + a_1a_2 + a_3 = \sigma_{\mathrm{ce}} \tag{6a}$$

$$\sigma(\varepsilon_{\mathrm{cu}}) = a_1\varepsilon_{\mathrm{cu}}^2 + 2a_1a_2\varepsilon_{\mathrm{cu}} + a_1a_2 + a_3 = \sigma_{\mathrm{cu}} \tag{6b}$$

$$\frac{d\sigma(\varepsilon_{\mathrm{cu}})}{d\varepsilon} = 2a_1\varepsilon_{\mathrm{cu}} + 2a_1a_2 = 0 \tag{6c}$$

where a_i (i = 1, 2, 3) are coefficients, ε_{cu} is the maximum strain in the compressive loading ($\mu\varepsilon$), and ε_{ce} is the compressive strain at the point of proportional limit ($\mu\varepsilon$), σ_{ce} is the compressive strength at the point of proportional limit (MPa), and σ_{cu} is the maximum compressive strength of test material (MPa). Equation 6c represents the condition of the compressive curve turning from nonlinear hardening stage to nonlinear softening stage at the peak point. The coefficients can be determined by solving Eq. 6, yielding Eq. 7a, 7b, and 7c,

$$a_1 = -\frac{\sigma_{cu}-\sigma_{ce}}{(\varepsilon_{cu}-\varepsilon_{ce})^2} \tag{7a}$$

$$a_2 = -\varepsilon_{cu} \tag{7b}$$

$$a_3 = \frac{\varepsilon_{ce}^2\sigma_{cu}-2\varepsilon_{ce}\varepsilon_{cu}\sigma_{cu}+\varepsilon_{cu}^2\sigma_{ce}}{(\varepsilon_{cu}-\varepsilon_{ce})^2} \tag{7c}$$

where ε_{cu} is the maximum strain in the compressive loading ($\mu\varepsilon$), and ε_{ce} is the compressive strain at the point of proportional limit ($\mu\varepsilon$), σ_{ce} is the compressive strength at the point of proportional limit (MPa), and σ_{cu} is the maximum compressive strength of test material (MPa).

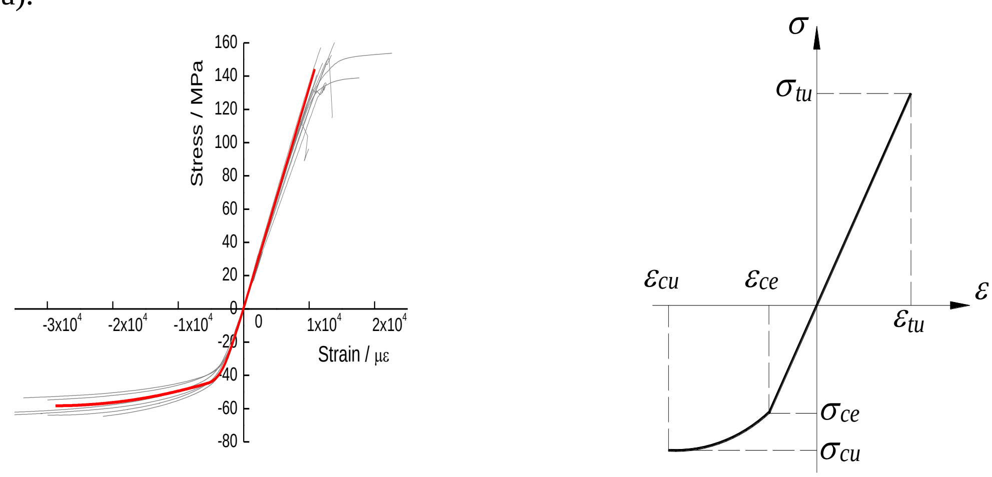

(a) Comparison of experimental and analytical curves **(b)** Analytical curves

Fig. 5. The longitudinal stress-strain relationships of PSB

Substituting the mean values of the stress and strain from Table 3 into Eq. 7a, 7b, and 7c gave the values a_i (i = 1, 2, 3) and upon substituting a_i (i = 1, 2, 3) to Eq. 6a, 6b, and 6c, the stress-strain relationship can be obtained, as the red line shown in Fig. 4b. It was observed that the curves obtained *via* calculations with Eq. 6a, 6b, and 6c agreed with those obtained *via* testing.

CONCLUSIONS

1. The tensile and compressive moduli of parallel strand bamboo (PSB) composites were found to be essentially identical. The tensile strength, however, was far greater than the compressive strength; the tensile failure was due to the breaking of the longitudinal fibers and showed brittle characteristics.

2. The stress-strain relationship in the longitudinal direction for PSB composites exhibited linear behaviour for tension, as well as for compression within the proportional limit; it exhibited nonlinear behaviour once the compressive stress went beyond the proportional limit.
3. Compressive failure had 3 modes; longitudinal buckling failure, compressive-shearing failure, and longitudinally slip failure. General damage characteristics of compression were the buckling of the fibers near the crack.
4. The stress-strain relationship curves of the 3 failure modes were almost identical; the compressive stress-strain relationship exhibited linear stage and nonlinear hardening stage within and beyond the proportional limit. The nonlinearity of the compressive stress-strain curve can be simulated *via* quadratic polynomial.

ACKNOWLEDGMENTS

This work was supported by the National Key Research Project (No. 2017YFF0207203-04), the Priority Academic Program Development of Jiangsu Higher Education Institutions (PAPD), and the Doctorate Fellowship Foundation of Nanjing Forestry University.

REFERENCES CITED

ASTM D143 (2014). "Standard test method for small clear specimens of timber," ASTM International, West Conshohoken, PA, USA.

Chen, G., Li, H. T., Zhou, T., Li, C. L., Song, Y. Q., and Xu, R. (2015). "Experimental evaluation on mechanical performance of OSB webbed parallel strand bamboo I-joist with holes in the web," *Construction and Building Materials* 101, 91-98. DOI: 10.1016/j.conbuildmat.2015.10.041

Chun, G. D. (2016). "A study on sliced bamboo veneer-Chinese fir glulam composite panel," *Advanced Materials Research* 1068(338), 2033-2036. DOI: 10.4028/www.scientific.net/AMR.168-170.2033

Chung, K. F., and Yu, W. K. (2002). "Mechanical properties of structural bamboo for bamboo scaffoldings," *Engineering Structures* 24(4), 429-442. DOI: 10.1016/S0141-0296(01)00110-9

Gou, C., Bo, S., and Yan, X. (2011a). "Aseismic performance tests for a light glulam house," *J. Vibration Shock* 30(10), 136-142. DOI: 10.3969/j.issn.1000-3835.2011.10.026

Gou, C., and Yan, X. (2011b). "Experimental study and engineering application of bamboo roof truss," *Industrial Construction* 43(8), 69-74. DOI: 10.7617/j.issn.1000-8993.2013.08.015

Huang, Y. S., Yu, S. L., Zhen, W. Z., and Tian, Y. (2010). "Application and prospect of bamboo/steel composite material in civil engineering structure," *Advanced Materials Research* 956(229), 989-993. DOI:10.4028/www.scientific.net/AMR.113-116.989

Huang, D. S., Zhou, A. P., and Bian, Y. L. (2013). "Experimental and analytical study on the nonlinear bending of parallel strand bamboo beams," *Construction and Building Materials* 44, 585-592. DOI: 10.1016/j.conbuildmat.2013.03.050

Li, Q., Tang, X. M., Li, N., Xian, Z. Y., Zhang, H. M., and Luo, J. J. (2009). "Study on technology optimization for the manufacture of molded panel with bamboo strands," *Guangxi Forestry Science* 38(1), 31-34. DOI: 10.3969/j.issn.1006-1126.2009.01.008

Li, Q., and Wang, K. H. (2001). "Research on the manufacture process of reformed bamboo," *China Wood-based Panels* 7, 6-9. DOI: 10.3969/j.issn.1673-5064.2001.07.002

Li, Y., Sheng, H., Shan, W., and Han, T. (2012). "Flexural behavior of lightweight bamboo-steel composite slabs," *Thin Wall Structures* 53, 83-90. DOI: 10.1016/j.tws.2012.01.001

Lo, T. Y., Cui, H. Z., and Leung, H. C. (2004). "The effect of fiber density on strength capacity of bamboo," *Materials Letters* 58(21), 2595-2598. DOI: 10.1016/j.matlet.2004.03.029

Lo, T. Y., Cui, H. Z., Tang, P. W. C., and Leung, H. C. (2008). "Strength analysis of bamboo by micros2008copic investigation of bamboo fiber," *Construction and Building Materials* 22(7), 1532-1535. DOI: 10.1016/j.conbuildmat.2007.03.031

Lu, Q. F., Wei, Y., Zhang, Q. S., Yu, Y. Z., and Lu, Z. T. (2008). "Experimental study on mechanical properties of basic components for a new anti-seismic room with bamboo engineering materials," *Research & Application of Building Materials* 11, 1-5. DOI: 10.3969/j.issn.1009-9441.2008.11.001

Wei, Y., Jiang, S. X., Lu, Q. F., Zhang, Q. S., Wang, L. B., and Lu, Z. T. (2010). "Experimental study on flexural performance of bamboo beams," *Building Structure* 40(1), 88-91. DOI: 10. 19701/j.jzjg.2010.01.025

Wei, Y., Zhang, Q. S., Jiang, S. X., Lu, Q. F., Lu, Z. T. (2011). "Basic properties and prospects of modern bamboo engineering materials applied in building structures," *Architecture Technology* 42(5), 390-393. DOI: 10.3969/j.issn.1000-4726.2011.05.001

Xiao, Y., and Ma, J. (2012). "Fire simulation test and analysis of laminated bamboo frame building," *Construction and Building Materials* 34, 257-266. DOI: 10.1016/j.conbuildmat.2012.02.077

Xiao, Y., She, L. Y., and Shan, B. (2009). "Research and design of prefabricated bamboo house," *Industrial Construction* 39(1), 56-59. DOI: 10.13204/j.gyjz2009.01.013

Xiao, L. X., Xiao, J. H., Hu, X. S., and Wang, S. H. (2005). "Study on the present situation and development of bamboo industry in China," *World Bamboo and Rattan* 3(3), 29-32. DOI: 10.3969/j.issn.1672-0431.2005.03.008

Zhou, A. P., Huang, D. S., Li, H. T., and Su, Y. (2012). "Hybrid approach to determine the mechanical properties of fibers and matrixes of bamboo," *Construction and Building Materials* 35, 191-196. DOI: 10.1016/j.conbuildmat.2012.03.011

Article submitted: July 8, 2019; Peer review completed: September 3, 2019; Revised version received: October 3, 2019; Accepted: October 15, 2019; Published: October 21, 2019.
DOI: 10.15376/biores.14.4.9645-9657

APPENDIX

Supplementary

Table S1. Tensile Results

Number of specimens	Maximum strain($\mu\varepsilon$)	Maximum stress (MPa)	Moduli (GPa)	Number of specimens	Maximum strain ($\mu\varepsilon$)	Ultimate stress (MPa)	Moduli (GPa)
ZL-1	11775	97.63	9.77	ZL-18	12788	149.72	13.57
ZL-2	10952	105.05	11.00	ZL-19	13416	152.55	13.40
ZL-3	7977	132.99	17.23	ZL-21	9988	122.45	14.27
ZL-4	11958	146.99	13.87	ZL-22	9158	106.42	12.40
ZL-5	8849	112.73	13.93	ZL-23	10184	133.91	15.10
ZL-6	14234	163.79	12.90	ZL-25	14210	189.02	12.67
ZL-7	12404	139.32	11.90	ZL-26	8180	93.65	15.50
ZL-8	10595	103.83	11.00	ZL-27	7875	84.74	12.53
ZL-9	9000	93.98	11.73	ZL-28	10900	124.53	12.80
ZL-10	12338	135.26	12.50	ZL-29	12069	124.15	12.07
ZL-11	6789	78.58	12.27	ZL-30	11182	140.90	11.93
ZL-12	13501	136.56	11.53	ZL-31	10412	136.22	13.73
ZL-13	10356	127.37	13.73	ZL-32	13815	168.92	14.60
ZL-14	11078	95.02	11.07	ZL-33	12737	150.10	13.20
ZL-15	11780	157.22	14.70	ZL-34	13378	162.79	13.77
ZL-16	8708	112.88	14.80	ZL-35	12249	137.70	13.43
ZL-17	13173	106.14	9.87				

Table S2. Compressive Results

Number of specimens	Proportional strain limit ($\mu\varepsilon$)	Proportional stress limit (MPa)	Maximum strain limit ($\mu\varepsilon$)	Maximum stress limit (MPa)	Moduli (MPa)
U-2	5485.1	39.57	31181.6	55.05	12.88
U-3	4953.0	40.82	25272.3	58.19	13.15
U-4	4971.1	45.42	27312.1	66.29	13.52
U-5	5754.0	41.12	23498.2	57.23	11.30
U-6	4895.0	43.21	20432.4	58.24	14.12
U-7	4894.8	43.21	35337.9	63.74	13.45
U-8	5682.5	44.25	32908.0	61.73	12.30
U-9	5079.5	37.21	16113.9	49.31	11.37
U-10	5391.5	45.27	40024.4	66.38	13.07
M-1	3119.5	28.73	29978.9	47.76	12.25
M-2	4062.0	27.48	26011.6	41.50	10.90
M-3	4062.5	27.48	27456.6	41.12	10.80
M-4	5381.5	53.74	9265.2	63.14	14.70
M-5	3259.5	27.47	26070.1	44.43	12.00
A-1	4833.0	39.44	20834.6	53.00	13.06
A-2	4995.5	36.99	23779.0	51.43	13.53
A-3	4578.5	37.78	33698.9	53.48	13.00
A-4	4875.5	39.04	16960.8	50.76	13.10
A-5	3875.0	39.15	19643.9	55.34	14.13
D-1	6326.0	46.98	11215.9	58.00	11.8
D-3	6099.5	46.59	24143.4	63.65	11.3
D-4	5152.0	42.61	17838.6	57.29	11.7
D-5	5642.5	41.96	35524.5	62.42	12.1
D-6	5527.5	42.84	28123.8	61.57	10.8
D-7	5648.5	45.25	29929.1	63.90	11.7
D-8	4928.5	39.06	14608.9	51.94	11.6
D-9	5529.0	46.10	17838.6	65.43	11.3
D-10	5086.5	38.92	13979.6	51.90	11.4